Journal of Materials Science: Materials in Medicine (2020) 31:1
https://doi.org/10.1007/s10856-019-6328-5

BIOCOMPATIBILITY STUDIES

Original Research

# Assessing two-way interactions between cells and inorganic nanoparticles

C. Cristallini[1] · N. Barbani[1,2] · S. Bianchi[3] · S. Maltinti[2] · A. Baldassare[2] · R. Ishak[2] · M. Onor[4] · L. Ambrosio[5] · V. Castelvetro[3] · M. G. Cascone[2,6]

Received: 13 June 2019 / Accepted: 16 November 2019 / Published online: 5 December 2019


## Abstract

A safe and effective use of nanoparticles in biology and medicine requires a thorough understanding, down to the molecular level, of how nanoparticles interact with cells in the physiological environment. This study evaluated the two-way interaction between inorganic nanomaterials (INMs) and cells from A549 human lung carcinoma cell line. The interaction between silica and zinc oxide INMs and cells was investigated using both standard methods and advanced characterization techniques. The effect of INMs on cell properties was evaluated in terms of cell viability, chemical modifications, and volume changes. The effect of cells and culture medium on INMs was evaluated using dynamic light scattering (DLS), scanning electron microscopy and energy-dispersive X-ray spectroscopy (SEM–EDS), high performance liquid chromatography (HPLC), gas chromatography-mass spectroscopy (GC–MS), Fourier transform infrared spectroscopy (FTIR), and thermogravimetric analysis (TGA). No cytotoxic effect was detected in the case of silicon oxide INMs, while for high doses of zinc oxide INMs a reduction of cell survival was observed. Also, increased cell volume was recorded after 24 h incubation of cells with zinc oxide INMs. A better dimensional homogeneity and colloidal stability was observed by DLS for silicon oxide INMs than for zinc oxide INMs. SEM–EDS analysis showed the effectiveness of the adopted dispersion procedure and confirmed in the case of zinc oxide INMs the presence of residual substances derived from organosilane coating. HPLC and GC–MS performed on INMs aqueous dispersions after 24 h incubation showed an additional peak related to the presence of an organic contaminant only in the case of zinc oxide INMs. FTIR Chemical Imaging carried out directly on the cells showed, in case of incubation with zinc oxide INMs, a modification of the spectra in correspondence of phospholipids, nucleic acids and proteins characteristic absorption bands when compared with untreated cells. Overall, our results confirm the importance of developing new experimental methods and techniques for improving the knowledge about the biosafety of nanomaterials.

✉ C. Cristallini
caterina.cristallini@cnr.it

[1] Institute for Chemical and Physical Processes, IPCF ss Pisa, CNR, c/o Largo Lucio Lazzarino, 56126 Pisa, Italy

[2] Department of Civil and Industrial Engineering, DICI, University of Pisa, Largo Lucio Lazzarino, Largo Lucio Lazzarino, 56126 Pisa, Italy

[3] Department of Chemistry and Industrial Chemistry, DCCI, University of Pisa, via Giuseppe Moruzzi, 13, 56124 Pisa, Italy

[4] Institute of Chemistry of Organometallic Compounds, ICCOM uos Pisa, CNR, via Giuseppe Moruzzi, 1, 56124 Pisa, Italy

[5] Institute for Polymers, Composites and Biomaterials, IPCB, CNR, via Campi Flegrei, 34, 80078 Pozzuoli, NA, Italy

[6] Inter-University Center for the 3Rs Principles in Teaching & Research (Centro 3R), Pisa, Italy

## 1 Introduction

In recent decades, the use of nanotechnology has increased dramatically in various fields including optics, electronics, energy conversion, personal care, and medicine. The most important medical applications of nanotechnology are in clinical diagnostic imaging and drug delivery systems [1–4].

Nanotechnology entails the controlled synthesis of materials having an ultra-small size, comparable to natural biomacromolecules and cellular nanostructures. The most widely studied class of nanomaterials is nanoparticles (NPs), thanks to the ease and efficiency of their production from a variety of materials. Very promising appears the role of NPs in the controlled delivery and targeting of pharmaceutical and diagnostics agents for cancer treatment.

Research efforts focus increasingly on NPs based on inorganic materials (INMs): gold NPs, quantum dots, silica NPs, iron oxide NPs, carbon nanotubes, and other metal oxide NPs, have emerged as promising alternatives to organic systems for a wide range of biomedical applications [5–7]. Compared to their micron-sized bulk counterparts, nanoparticles present a higher surface/volume ratio [8] maximizing the possibility to load them with therapeutic drugs, and to deliver these agents to target cells and tissues. In addition, nanoparticles can pass through physiological barriers and penetrate deeply into tumor sites where they are retained by a process recognized as enhanced permeation and retention (EPR) effect [9, 10]. Recent in vitro observations indicate that certain types of metal oxide nanoparticles can preferentially kill cancer cells with strikingly lower toxicity against normal cells. Zinc oxide nanoparticles, for instance, exhibit a high degree of cancer cell selectivity, and exceed the therapeutic indices of some commonly used chemotherapeutic agents [11, 12].

Although nanoparticles can be produced using many different materials, concerns about their compatibility with living cells limit the types of nanomaterials currently under consideration for use in biomedical applications. A more thorough and in-depth investigation about the cytotoxicity of nanomaterials is required prior to their translation in biomedicine [13].

The assessment of safety and impact of nanomaterials on human health must be performed in accordance with regulatory issues. It is critical to provide legislators with a set of tools for reliable and exhaustive risk assessment; including new testing strategies, adapted to a wide range of nanomaterials, and broadly accepted datasets. In particular, in vitro methodologies providing predictive values for regulatory purposes should be identified and used as an alternative strategy for risk assessment in the direction of replacing animal tests [14]. Advanced physico-chemical characterization techniques and suitable cell lines must be investigated for in vitro cytotoxicity assessments of nanomaterials with different size and chemical composition.

In particular, it is crucial to unravel the interactions occurring at the molecular level between nanomaterials and living cells. Studies evaluating the toxicity of nanomaterials (NMs) on mammalian cells have produced contradictory results [15–17].

Various studies have shown that zinc oxide nanoparticles could directly damage pulmonary system [18] and can induce oxidative stress, inflammation and DNA damage in cell and animal models [19].

Most studies focused on the role of particle size and of other parameters such as particle composition, agglomeration and production methods. It is generally agreed that the size of nanoparticles is negatively correlated with their toxicity.

It was found that zinc oxide particles with smaller size are more toxic than same particles with a larger size at the same dosage applied in cultured cell models [20]. A recent study [21] showed that 50 nm zinc oxide nanoparticles induced severe A549 cell death, while 200 nm zinc oxide nanoparticles induced A549 cell death at a less extent degree.

With regard to silica nanoparticles the extent and mechanism of their cytotoxicity were found to be not only size and dose dependent but also highly cell type dependent. HepG2 cells resulted the least susceptible to the toxic effects of silica nanoparticles while NIH/3T3 cells were clearly the most susceptible. High doses of 60 nm silica nanoparticles significantly reduced cell viability in three different cell types (HepG2, NIH/3T3, and A549). 60 nm SNPs affected cells much differently than nanoparticles of other sizes, most likely due to enhanced uptake.

60 nm silica nanoparticles were preferentially endocytosed by cells but at high doses caused a decrease in cell viability. Therefore these particles may be ideal for biomedical applications requiring cellular uptake but fatal at high doses [22].

The present study is part of the European Project NANoREG aimed at determining the most appropriate ways to assess the environmental, health, and safety effects of nanomaterials.

Aim of the study is a comprehensive evaluation of the two-way interactions between cells and inorganic nanoparticles from a morphological, physico-chemical and biological point of view, using several methods and advanced techniques. A549 cells were selected, as cell model, for their well-established use in toxicology and more recently in pulmonary drug delivery strategies [23]. Nanomaterials based on zinc oxide (NM111) and silica (NM203) were employed and their effect on the cell properties was evaluated in terms of: (i) cell viability, by in vitro MTS assay; (ii) chemical modifications using FTIR Chemical Imaging; (iii) dimensional change using the Scepter 2.0 cell counter. The effect of the cells on INMs was evaluated by dimensional-morphological analysis (DLS and SEM), by chemical analysis using HPLC, GC–MS and FTIR, and by thermal analyses. The MTS assay and DLS analysis were carried out using harmonized protocols (NANoREG).

## 2 Materials and methods

### 2.1 Materials

Inorganic nanoparticles of silica (fumed $SiO_2$, NM203) and zinc oxide (precipitated ZnO with hydrophobic organic coating, NM111) were obtained from the European Commission's Joint Research Centre (JRC) and identified as

JRCNM01101 (73 nm diameter primary particles with hexagonal zincite crystal structure, 141 nm mean diameter as measured by TEM analysis, aggregates/agglomerates in aqueous dispersion with reported 253 nm z-average diameter and broad polydispersity as measured by DLS) and JRCNM02003 (amorphous silica obtained by $SiCl_4$ combustion, 24.7 nm diameter primary particles, aggregates/agglomerates in aqueous dispersion with reported 176 nm z-average diameter and broad polydispersity as measured by DLS, zeta potential $\zeta \sim -35$ mV at pH = 7), respectively [24].

Cells from an A549 human lung carcinoma cell line, employed for MTS assay and physico-chemical characterization, were provided by BAuA (Bundesanstalt Fuer Arbeitsschutz und Arbeitsmedizin, Germany). The following products were utilized: MEM-GlutaMAX culture medium, 5 µg/mL streptomycin–penicillin (Gibco by Life Technologies Corporation, Paisley, UK); Fetal Bovine Serum (FBS), Bovine Serum Albumin (BSA), trypsin 0.05 % EDTA solution, and Dulbecco's phosphate buffered saline (PBS) (Sigma Aldrich, St. Louis, MO); CellTiter 96 Aqueous One Solution Cell Proliferation Assay (MTS) (Promega Corporation, Madison, USA); ethanol (EtOH) (Carlo Erba Reagenti, Italy).

## 2.2 Preparation of INMs batch dispersions

Nanoparticle stock dispersions for in vitro cytotoxicity analysis were prepared by ultrasonication (according to the NANoREG protocol). In a sterile laminar flow hood, a 0.05 % (w/v) BSA aqueous solution was prepared as dispersion medium. Pre-weighed amounts (15.36 mg) of NM203 and NM111 were inserted directly into clean vials, then 30 µL EtOH were added to each vial, followed by 970 µL of the 0.05% BSA solution. EtOH and BSA were introduced mainly to improve the dispersion of NM111, having a hydrophobic alkylsilane coating. A 5 mL volume of MilliQ water was added by pipetting along the vial sidewalls to obtain INMs dispersions with a final concentration of 2.56 mg/mL. The vials were placed in an ice water bath, then a sonicator probe (13 mm diameter, model dr Hielscher UP400s) was inserted for about one third into each dispersion. Sonication was performed in continuous mode for 12 min at 20% amplitude of the 460 $W/cm^3$ nominal acoustic power density.

## 2.3 Cell viability test

Complete culture medium (CCM) was prepared using MEM-GlutaMAX supplemented with fetal bovine serum (FBS) (10%) and penicillin/streptomycin (5 µg/mL). The medium was sterile filtered using a Nalgene vacuum filtration system (Sigma). A549 cells were grown in CCM in 75 $cm^2$ flasks, changing the medium every 3 days. After reaching 90% confluence, they were trypsinized and seeded in 96-well plates, at a density of $1 \times 10^4$ cells/well, to perform the MTS test.

Three independent MTS assays were performed, each in triplicate, according to the NANoREG protocol. Cell viability was assessed after 24 h incubation with NM11or NM203, both used at five different concentrations: 100, 50, 25, 10, and 1 µg/mL. Aqueous $CdSO_4$ solutions at five different concentrations (150, 125, 100, 75, and 37.5 µM) were used as positive control.

The cell survival percentage (CS%) was calculated as follows: CS% = (individual absorbance of treated cells/average absorbance of untreated cells) × 100. The raw data obtained for each plate were analyzed. The values of EC50 were calculated for both types of INMs using a logistic fit of the CS% values obtained from the three replicates at various concentrations.

## 2.4 Cell culture for chromatographic analysis, FTIR, and Scepter analysis

### 2.4.1 Cell cultivation

Complementary analyses (HPLC, GC–MS, FTIR, and Scepter analysis) were carried out on both culture medium and cells after 24 h incubation with INMs.

Doses of INMs and cell seeding densities were selected in order to compare the results of these tests with that of the MTS viability test. Batch dispersions of INMs were added, 24 h after seeding, to the cells cultured in a 48-well plate. After 24 h incubation, the supernatant was completely removed from each well and used for chromatographic tests, while the cells were detached from the wells by treatment with trypsin-0.05% EDTA solution and used for Scepter and FTIR Chemical Imaging analyses.

### 2.4.2 Analysis by Scepter cell counter

The effect on cell volume of both NM203 and NM111 was evaluated using a Scepter 2.0 Cell Counter, the device has sensors allowing rapid cell counting and giving quantitative information on cell concentration, volume, and diameter 0.60 µm sensors were used, compatible with the size of the employed cell type.

After 24 h incubation with INMs, the cells were washed three times using sterile PBS to remove INMs completely and then trypsinized using a trypsin-0.05% EDTA solution. After trypsinization, the obtained cell suspension was transferred into a 15 mL centrifuge tube and centrifuged at 1200 rpm for 5 min. The supernatant was removed and the cells were re-suspended in 1 mL of fresh CCM. A sample was prepared for cell counting by diluting 20 µL of cell

suspension with PBS to a final volume of 100 µL inside a vial. Then, the Scepter sensor was introduced into the vial and the sample was drawn by pipetting once.

## 2.5 Dimensional and morphological analysis

### 2.5.1 DLS analysis

Hydrodynamic size (z-average ± SD) and polydispersity index (PDI) of IMNs were determined by dynamic light scattering (DLS) using a Zetasizer Malvern nano ZS90. A general procedure was followed according to the NANoREG protocol. The measurements were carried out at two different temperatures: at 25 °C on the INMs batch dispersions, and at 37 °C on the INMs dispersions in culture medium at two different concentrations (10 and 100 µg/mL) both at initial time (t0) and after 24 h incubation (t24).

### 2.5.2 SEM–EDS analysis

Scanning electron microscopy and energy-dispersive X-ray spectroscopy (SEM–EDS) were employed to analyze INMs in form of raw materials and batch dispersions, using a FEI Quanta™ 450 FEG instrument. SEM analysis was done at 15 kV in high-vacuum mode, with manual aperture, 2.5 beam spot size, ×120,000 magnification and horizontal field width (HFW = 3.45 µm). The INMs were immobilized on Si-free carbon tape and sputtered with gold to improve the quality of the analyses. X-ray microanalysis (EDS) was performed to analyze chemical composition and check for the presence of organic contaminants.

## 2.6 FTIR analysis

FTIR analysis in ATR mode (Spectrum 400, Perkin Elmer) was performed on the INMs as pristine powders, after contact with the dispersion medium (0.05% BSA-water solution), upon incubation with the culture medium at initial time (t0) and after 24 h (t24), and after thermogravimetric analysis (TGA).

Thermogravimetric analysis (TGA-6, Perkin Elmer) was carried out on samples of ca. 10 mg heated from 25 to 800 °C at a rate of 10 °C/min with a nitrogen purge.

Chemical analysis was carried out by FTIR Chemical Imaging (Perkin Elmer Spotlight 300). Spectral images were acquired in transmission mode (spectral resolution 6 $cm^{-1}$, spatial resolution 20 µm × 20 µm).

FTIR analysis was performed directly on the cells after incubation with INMs following the procedure described above and specially designed for this purpose according to literature [25]. After 24 h incubation with INMs, cells were collected using trypsin-0.05% EDTA solution, subjected to several PBS washings, centrifuged, seeded on a $BaF_2$ (13 mm × 2 mm) plate, air dried for 5 min, and analyzed.

The recorded spectral maps were elaborated using the Spotlight 300 software to produce a correlation map and a band absorbance ratio. The correlation map shows the areas of an image where spectra are most similar to a reference spectrum. Band ratio analysis is commonly used for quantification in infrared spectroscopy. This involves the measurement of either the peak absorbance or the band area of an internal reference, with respect to the corresponding values of a band of interest. The Spotlight software was used to evaluate the presence and distribution of different components and obtain chemical and correlation maps. The use of second derivative and smoothing procedures of the spectral maps provided more detailed information regarding the protein secondary structure.

## 2.7 Chromatographic analysis

Release tests were performed using high-performance liquid chromatography (HPLC, Perkin Elmer Series 200) and gas chromatography coupled with mass spectrometry (GC–MS, Agilent 7890A-5975C). INMs were placed in tubes containing MilliQ water at 37 °C, under constant stirring. After 24 h, the supernatant was collected and analyzed to identify released substances. Moreover, as previously described, the supernatants withdrawn from cell plates treated with INMs were first diluted with MilliQ water and desalted with Amberlite resins, then centrifuged and filtered through 0.2 µm cellulose acetate filters. For HPLC analysis the supernatants were placed into 1.5 mL HPLC vials. A 100 µl aliquot of filtrate from each sample was then injected into the HPLC system. For HPLC analysis, a C18 Phenomenex column, acetonitrile/MilliQ water 80/20 as the mobile phase, UV detector set at 210 nm wavelength, and 1 mL/min eluent flow rate were used. GC–MS data were obtained using an Agilent 7890A gas chromatograph equipped with an Agilent 5975c mass spectrometer detector and a CTC CombiPAL autosampler with SPME fiber. 1 mL of each sample in a 10 mL headspace vial (Agilent, P/N 8010-0139) was incubated at 50 °C for 10 min following 5 min of preconcentration on PDMS-Carboxen SPME fiber of headspace. The inlet was kept at 280 °C and the fiber was desorbed for 10 min at a flow rate of 1 mL/min. The oven was held at 30 °C for 6.5 min and then ramped to 240 °C at 8 °C/min. GC separation was carried out on a high-polarity column (DB-FFAP nitroterephthalic acid modified polyethylene glycol column: 60 m length, 0.250 mm ID, 0.50 m lm). The transfer line was set at 230 °C.

## 2.8 Statistical analysis

Acceptance criteria for MTS tests included the following conditions: the coefficient of variation of the average

absorbance (Absc) of untreated cells had to be lower than 30% in all the experiments; the difference between the Absc of the cells in untreated wells and Absc of the treated cells had to be lower than 15%; the coefficient of variation of Absc of technical replica measurements must be lower than 30% for INMs; at least one concentration of the applied $CdSO_4$ doses must have a CS% < 70.

The values of half maximum effective concentration (EC50) was calculated using GraphPad Prism software of CS% values at 0–100 µg/ml concentrations ($n = 3$).

For FT-IR results a statistical analysis was performed by Principal Component Analysis (PCA). This is a powerful method for the analysis of large spectral data sets. It gathers the spectra in data groups of similar multi-parameter variability and allows the identification and differentiation of dissimilar spectral groups, such as data sets corresponding to different samples or regions of samples. Scatter plots were drawn to identify clusters of data more significantly associated with cells (positive score).

## 3 Results and discussion

### 3.1 Cell viability tests

Assessing the effect of size and composition of NMs on cellular metabolic activity is very important for specific cell lines (i.e. lung epithelial cells and monocytes), which are considered key cell types for toxicological responses to NMs.

To accurately evaluate the biosafety of NMs, in vitro toxicological tests must be carried out according to specific requirements and protocols in combination with a minimum set of NMs characterizations in order to compare the results with those obtained by other research groups on the same materials and using the same assays. In this work, we examined the effect of ZnO and $SiO_2$ INMs on cell viability. Dose-dependent cytotoxicity was analyzed using cells of A549 line according to a specific culture protocol in which different procedural steps and experimental parameters (i.e. cell concentration, time, reagents, positive control, culture medium composition) are well described, to ensure high quality of measurements and maximum data reproducibility. First, the quality and stability of INMs dispersions were optimized with respect to a silica standard nanomaterial. INMs were sonicated according to the NANoREG protocol in order to define the optimal parameters for the apparatus used in this work, through the calibration of the delivered acoustic power and of the de-agglomeration efficiency.

Figure 1 shows percent cell survival rates (CS%) measured in the presence of the two different types of INMs during three performed independent experiments.

In general, good agreement was observed among MTS results for NM203 in the different experiments. For all tested concentrations of NM203, the CS% values were close to 100% (Fig. 1a).

On the other hand, in the NM111cytoxicity tests, CS% results were consistently within a very low range (0–18%) at the highest INMs concentrations (100 µg/mL and 50 µg/mL, respectively) while for lower doses of NM111 (1, 10, and 25 µg/mL) CS% was very high in all experiments (>90%). These results indicate a toxic effect exerted by this kind of INMs on A549 cells, but only at high doses. Considering the positive control, the measured CS% values were low (2–28%) for all the experiments with the highest $CdSO_4$ concentration (150 µM), indicating a toxic effect of $CdSO_4$ at this concentration and confirming that the effect of $CdSO_4$ on the cells is concentration dependent.

Our results meet the acceptance criteria of the NANoREG protocol followed in all the experiments, confirming the validity of our method.

At the end of the exposure, cells cultured in untreated wells were viable, showing no evidence of cytotoxicity in all experiments. The coefficient of variation of the average absorbance (Absc) of untreated cells resulted lower than 30% for both NM203 and NM111 in all the experiments. The difference between the Absc of the cells in untreated wells and Absc of the treated cells was lower than 15% for both INMs. The coefficient of variation of Absc of

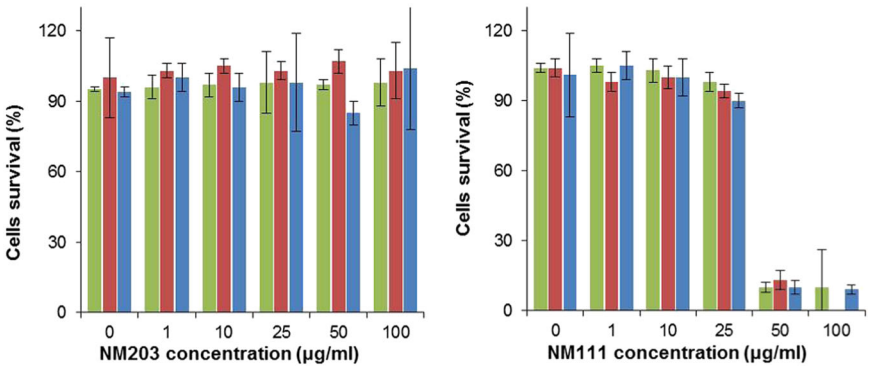


**Fig. 1** MTS analysis of cell viability upon treatment with 0, 1, 10, 25, 50, 100 µg/mL of (**a**) NM203 and (**b**) NM111 in A549 cells. CS% values are obtained from three independent experiments ($n = 3$ for each group) and values are expressed in mean ± SE

technical replica measurements resulted lower than 30% for both INMs. Finally, CS% in the wells containing positive control ($CdSO_4$) at 75 and 150 µM concentrations, was lower than 70% for all the experiments and for both NM203 and NM111. This is in accordance with the criteria for which at least one of the applied $CdSO_4$ doses must have a CS% < 70.

The values of half maximum effective concentration (EC50) for NM111 obtained in three different experiments and calculated using a logistic fit of CS% values (obtained from three replicates at various concentrations) were 31.27, 38.34, and 27.85 µg/mL, respectively. These results confirm the reproducibility of MTS data for both NM203 and NM111; in addition, NM203 results are in agreement with a previous study based on the MTT test [26]. On the contrary, a dose-dependent cytotoxic effect of NM111 was detected, differently from previous MTT results for this nanomaterial [26]. Such apparently inconsistent results may be due to impurities or contaminants in the silane coated NM111 sample used in this work. Indeed, the association with organic toxic substances is one of the possible issues to be checked by nanotoxicological assays.

A recent study [27] showed the dose dependent cytotoxicity of ZnO nanoparticles against A549 cells with a TC50 value of 35.7 µg/mL, which is comparable to EC50 values obtained by us for NM111 (28.75–38.34 µg/mL). A previous study demonstrated that ZnO nanoparticles induced significant oxidative stress-related cytotoxicity and genotoxicity in human lung fibroblasts in vitro and in D. melanogaster in vivo. In particular, cell viability was consistently found to be significantly decreased as early as 24 h after treatment, and ZnO nanoparticles at a concentration of 50 µg/mL caused total cell death [28].

**Table 1** Hydrodynamic diameter values obtained by DLS analysis for NM203 and NM111 in three independent experiments (exp1, exp2, exp3). The analysis was carried out in batch dispersion (2.56 mg/ml) and in culture medium at 100 µg/ml (100) or 10 µg/ml (10) at initial time (t0) and after 24 h incubation (t24). Ten runs for each measurement were performed

| Sample | NM111 Z-ave diameter (nm) | NM203 Z-ave diameter (nm) |
|---|---|---|
| Batch dispersion_exp1 | 177.9 ± 3.4 | 197.2 ± 1.6 |
| Batch dispersion_exp2 | 294.2 ± 4.8 | 200.3 ± 1.9 |
| Batch dispersion_exp2 | 288.0 ± 3.0 | 211.3 ± 2.1 |
| 100_t0_exp1 | 353.1 ± 4.9 | 206.9 ± 1. 8 |
| 100_t0_exp2 | 309.8 ± 5.8 | 214.8 ± 2.3 |
| 100_t0_exp3 | 214.8 ± 8.1 | 217.1 ± 10.1 |
| 100_t24_exp1 | 343.7 ± 7.4 | 296.8 ± 8.9 |
| 100_t24_exp2 | 363.3 ± 16.5 | 269.7 ± 8.2 |
| 100_t24_exp3 | 194.4 ± 10.5 | 210.2 ± 8.7 |
| 10_t0_exp1 | 71.1 ± 32.2 | 47.6 ± 1.8 |
| 10_t0_exp2 | 143.9 ± 34.5 | 125.9 ± 3.9 |
| 10_t0_exp3 | 154.0 ± 31.7 | 84.9 ± 20.2 |
| 10_t24_exp1 | 154.7 ± 2.9 | 156.0 ± 1.8 |
| 10_t24_exp2 | 181.4 ± 4.4 | 175.5 ± 3.9 |
| 10_t24_exp3 | 172.6 ± 4.4 | 172.2 ± 3.5 |

## 3.2 DLS analysis

Additional information to complement MTS tests, regarding size and aggregation state of INMs under the same experimental conditions, was obtained by DLS. The analyses were performed on nanoparticle batch dispersions (the same used for MTS test) and on nanoparticle dispersions in culture medium, both at initial time (t0) and after 24 h (t24) incubation. Based on prior experiments, two different concentrations were selected, 100 µg/mL and 10 µg/mL. The 100 µg/mL dose corresponds to the highest concentration used in MTS assay. The 10 µg/mL dose was selected considering that the lowest dose used in MTS (1 µg/mL) did not give reliable DLS results.

DLS analysis, performed on NM203 batch dispersion, showed very similar Z-ave diameter values in the three independent experiments (Table 1). In the case of NM111 batch dispersion, the values from the three experiments were significantly different, indicating greater dimensional homogeneity and stability for the batch dispersion of silica oxide nanoparticles than for zinc oxide nanoparticles.

In the case of NM203, the values obtained after incubation in culture medium at 37 °C at the highest concentration (100 µg/mL) and at initial time (t0) (100-t0) were similar to those obtained for batch dispersion. On the contrary, after 24 h of incubation a Z-ave value higher than that found at t0 was found in the first two experiments.

The analyses carried out at lower concentration (10 µg/mL) and at the initial time (10-t0) showed in both experiments a reduction of the hydrodynamic diameter with respect to batch dispersion suggesting that dilution hinders the agglomeration of the particles. A diameter increase was observed after 24 h of incubation in culture medium. These results suggest that both dilution and incubation time affect nanoparticles agglomeration. Incubation time is know to affect surface adsorption of culture medium components [29].

In the case of NM111 the values obtained at t0 and t24 at higher concentration (100-t0) were higher with respect to that observed for batch dispersion, while maintaining a certain variability within the three experiments. Also, in the case of NM111 the same effects of the dilution and incubation time on size were observed. Dispersion in BSA

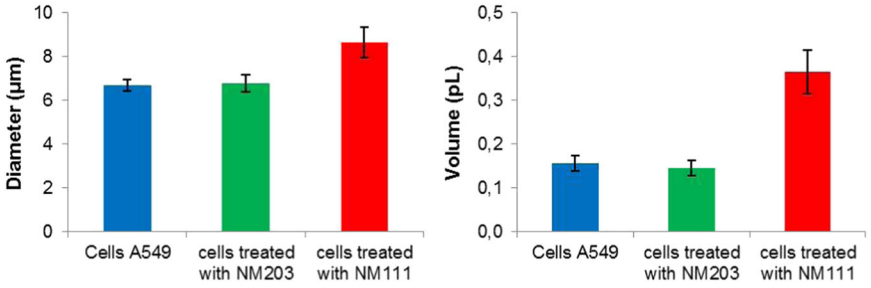


**Fig. 2** The effect on cell volume of INMs was evaluated using Scepter cell counter. Volume and diameter of A549 cells untreated and treated with 100 µg/ml of either NM203 or NM111. The device Scepter 2.0 cell counter has 60 µm sensor compatible with A549 cells. Values are means ± SE ($n = 6$)

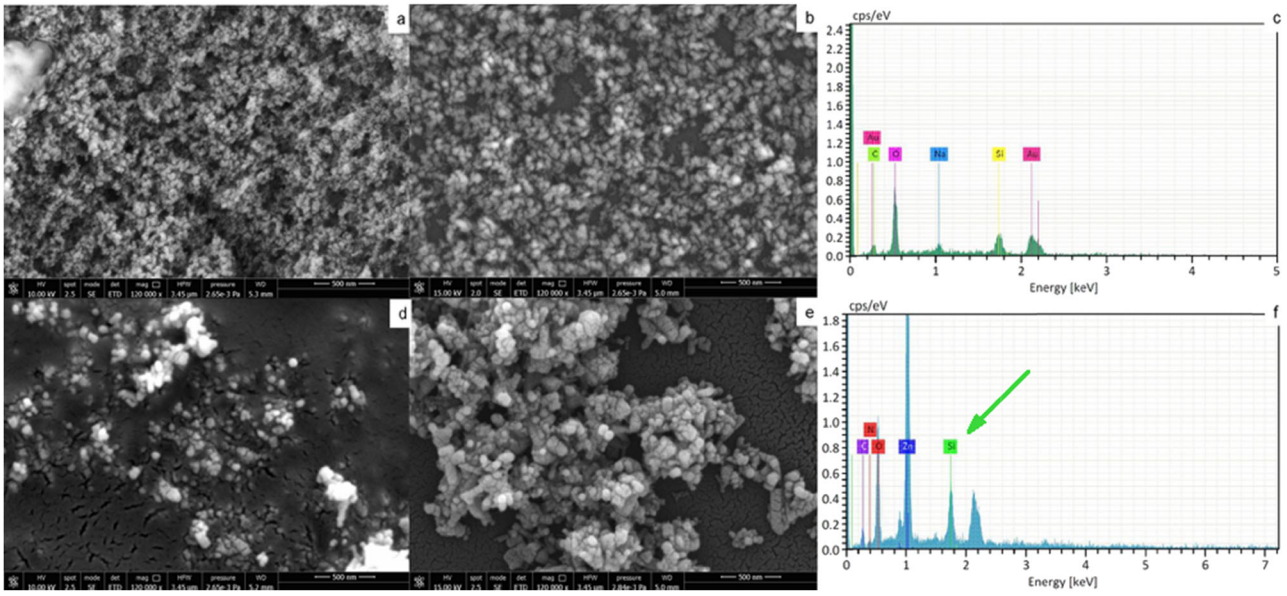


**Fig. 3** Results of SEM–EDS analysis performed on NM203 and NM111, both investigated as raw materials (**a, d**) and as deposited from batch dispersions (**b, e**). By comparing the images of the samples from the batch dispersions of both NM203 (**b**) and NM211 (**e**) with those from the raw materials (**a, d**) the effect of the adopted dispersion procedure can be observed. EDS spectra of NM203 batch dispersion (**c**) and zinc oxide batch dispersion (**f**) are compared and the presence of a peak from Si atoms is evident (indicated by an arrow) in the case of NM111(**f**) attributable to residual substances derived from the organosilane coating

solution and incubation in culture medium influenced the hydrodynamic diameter resulting above the nanometer scale.

### 3.3 Analysis by Scepter cell counter

In order to clarify the effect of particles on the cells, an evaluation of cell size after contact with INMs was performed with the Scepter cell counter. The Scepter cell counter is increasingly used for cell counting in vitro, as it yields more accurate results than visual counting or hemocytometry. Using the Scepter software, the counter also provides quantitative data on cell volume and size, in addition to relative concentrations [30].

Figure 2 shows volume and diameter of A549 cells both untreated and treated with the highest dose (100 µg/mL) of either NM203 or NM111. While an increase in both volume and diameter of the cells after treatment with NM111 is observed, contact of the cells with NM203 did not result in any measurable change compared to untreated cells. A variation in cell volume in the presence of zinc oxide nanoparticles may be due to cellular alteration: a volume increase is typical in the progression of a cell towards necrosis reflecting ion unbalance in the cytosol [31] caused by several factors related to the specific chemical structure or to the size of particle agglomerates.

### 3.4 SEM–EDS analysis

In Fig. 3 the results are reported of SEM–EDS analysis on samples NM203 and NM111 both as raw materials and as deposited from batch dispersions. By comparing the images of the samples from the batch dispersions with those from the raw materials, the effect of our dispersion procedure is observed. In the EDS spectrum of zinc oxide batch dispersion (Fig. 3f) the presence of a peak from Si atoms, not attributable to the carbon tape used as support for the particles, can be attributed to residual substances derived from the organosilane coating of NM111.

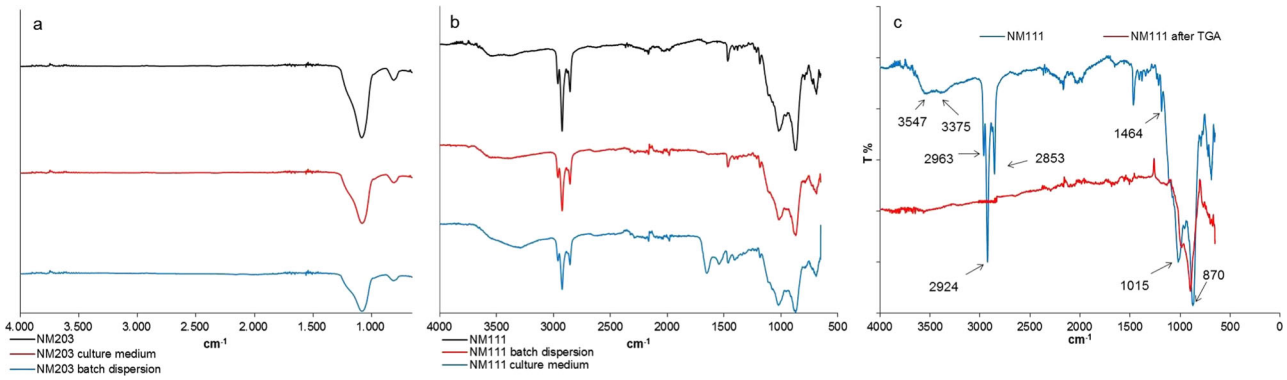


**Fig. 4** FTIR spectra were collected from the chemical maps obtained for untreated cells and cells after incubation with NM203 and NM111, respectively. The spectra of NM203 (**a**), NM111 (**b**), NM111 before and after TGA analysis (**c**) were analyzed, with particular reference to the characteristic bands listed in Table 2

### 3.5 Physico-chemical characterization

Considering that zinc oxide nanoparticles at high doses were found to produce a toxic effect on the cells according to the results of cell viability test, Scepter and EDS analysis, additional FTIR, TGA, and chromatographic analyses were carried out to investigate the presence of toxic substances released from the particles.

In the case of NM203 (Fig. 4a) the FTIR spectra of raw nanomaterial, INM batch dispersion and INM dispersion in culture medium, consistently show the characteristic Si-O absorptions at 1093 and 813 $cm^{-1}$, without any evident additional peak. On the contrary, in the case of NM111 (Fig. 4b) additional peaks, compared to those characteristic for the spectrum of zinc oxide INM (main absorption at 450 $cm^{-1}$, not visible in the explored spectral range), are present at 3547 (OH), 3375 (OH, NH), 2963, 2924, 2853 (CH stretchings), 1464 (CH bending), 1200, and 850 (Si–O groups) $cm^{-1}$. These can be associated to the presence of organosilane surface modifiers, as further confirmed by the FTIR spectra obtained from the same NM111 sample before and after thermogravimetric analysis (TGA). From the TGA thermogram (not shown) a total weight loss of 2–3 wt % occurs upon heating from 50 °C to 600 °C; the FTIR spectrum of the material collected from the crucible did not show any absorption in the 3500–1300 $cm^{-1}$ range, indicating complete pyrolytic removal of organic compounds, while the bands typical of silica or silica-like groups are present as in the pristine NM111 sample (spectrum in red in Fig. 4c). This agrees with the previously reported results of EDS analysis performed on NM111 batch dispersion.

The FTIR spectrum of NM111 obtained after incubation of the particles in culture medium shows additional amide I and amide II bands, suggesting the occurrence of protein adsorption. This agrees with the prompt increase of hydrodynamic size occurring upon contact of NM111 with the culture medium, as detected by DLS analysis. Adsorption of proteins by NM111 may be due to its higher surface hydrophobicity compared to NM203.

HPLC analysis performed on the supernatants of INMs dispersions in MilliQ water after 24 h incubation to check for the possible presence of impurities loosely bound to the INMs evidenced an additional peak only in the case of NM111 (data not shown). HPLC analysis was carried out also on supernatants from culture of cells untreated and treated with the nanoparticles. The chromatographic profiles obtained for the samples treated with either NM203 or NM111 did not present any additional peak compared to those obtained for samples from untreated cells.

A GC–MS analysis was carried out to identify the additional component observed in the supernatant of the NM111 dispersion in MilliQ water. The GC–MS chromatogram reported in Fig. 5a shows the presence of an intense peak at 27.03 min r.t., its MS spectrum matching that of 1-octanal, or caprylaldehyde, from the software library of the MS instrument. Caprylaldehyde could result from partial degradation of the organosilicon surface modifiers previously detected through FTIR and EDS analyses on NM111. Actually, the Si–C bond is very stable and decomposes only under particularly drastic conditions, as opposed to the Si–OC groups that are easily hydrolyzed with formation of the parent alcohol and silanol. However, organosilicon species have been reported to undergo enzymatic degradation involving Si–C bond cleavage through an oxidative pathway [32, 33], eventually resulting in the formation of an aldehyde as the oxidized alkyl derivative. In Fig. 5b a representative GC–MS chromatogram of the supernatant obtained from a NM111 dispersion in culture medium shows a series of peaks corresponding to the numerous cell metabolites (including alcohols and ethyl acetate), while the peak at 27.03 is absent, suggesting metabolic degradation of caprylaldehyde through NADH-dependent enzymatic hydrogenation.

Of particular relevance is that caprylaldehyde, like most aldehydes, can lead to a toxic effect, thus indirectly

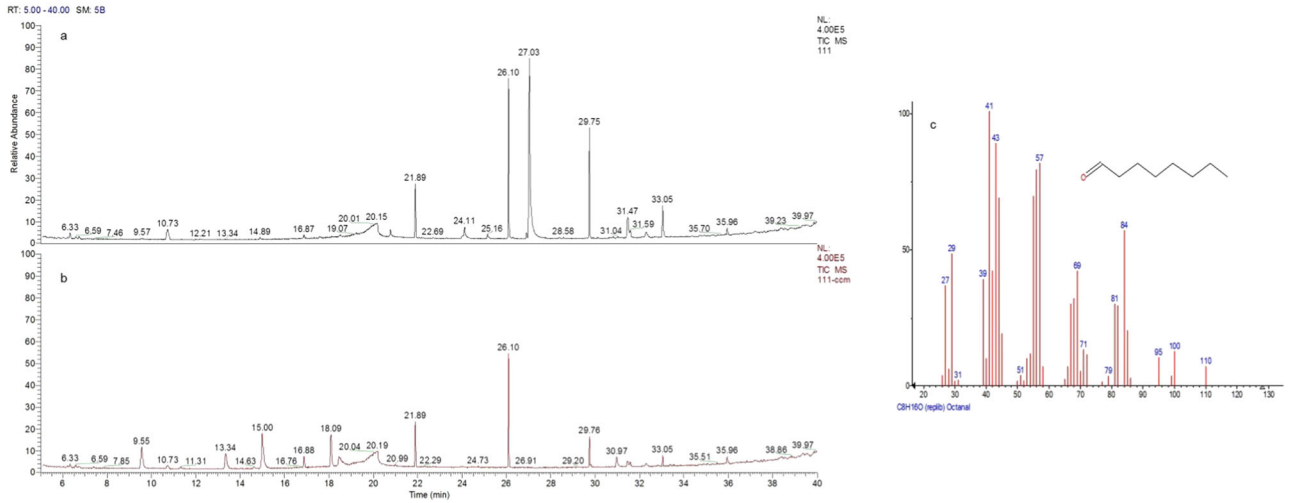


**Fig. 5** A GC–MS analysis was carried out to identify the additional component observed in the supernatant of the NM111 dispersion in MilliQ water. GC–MS profiles of supernatants are reported for NM111 in MilliQ water (**a**) and for NM111 in culture medium (**b**). The chromatogram of NM111 in water (**a**) shows an intense peak at 27.03 min r.t., matching the MS spectrum of 1-octanal. The chromatogram of NM111 in culture medium shows a series of peaks corresponding to the numerous cell metabolites (including alcohols and ethyl acetate), while the peak at 27.03 is absent

confirming the results obtained by MTS for this specific INM [18]. Recently, modification of mRNA expression in A549 human lung epithelial cells was demonstrated after in vitro exposure to octanal [34].

### 3.6 FTIR chemical imaging for cells

The molecular interactions occurring between the complex cell microenvironment and INMs were further investigated by FTIR Chemical Imaging, which is a useful tool for evaluating the effects exerted by INMs on cell biochemical composition [35]. One of the advantages of this technique is the possibility to directly analyze the biological samples without the need for staining procedures, thus reducing possible artifacts and allowing rapid sample analysis. FTIR spectroscopy is known for its unique sensitivity in identifying vibrational structures of biological materials [36]. A growing number of papers describe the use of FTIR to study protein conformation, nucleic acids and other cell components [37]. FTIR can be applied to the study of DNA damage at chemical bond level in cells [25]. In our case, FTIR was used for the identification of possible chemical alterations of protein and nuclear components as induced by the cell–INMs interaction. Figure 6 shows optical images and chemical maps of untreated cells, cells treated with NM111 and cells treated with NM203. The spectra acquired by the map of untreated cells show the typical bands associated with the cell's biomolecules. The frequency values, registered for the absorption bands, are in good agreement with values reported in the literature for healthy cells [38, 39].

From the chemical maps obtained for untreated cells and cells after incubation with NM203 and NM111, respectively, the spectra were obtained (Fig. 7a) and analyzed, with particular reference to the characteristic bands listed in Table 2. DNA spectral bands in the 980–1149 $cm^{-1}$ and 1151–1350 $cm^{-1}$ ranges are attributed to symmetric and asymmetric $PO_2$ stretching vibrations, respectively [36]. The typical bands of proteins are amide I at 1600–1700 $cm^{-1}$ and amide II at about 1550 $cm^{-1}$.

The second derivative spectra acquired from the map of untreated cells present the amide I absorption bands associated with the secondary structure of cellular proteins such as α-helical and β-turn conformations at 1685 (β-sheet), 1668 (β-turn), 1647 (α-helix), and 1630 (β-sheet) $cm^{-1}$ (Fig. 7b), in agreement with the secondary conformations that are normally present in the cellular proteins. The protein conformations detected from the second derivative spectra acquired from the map of cells treated with NM203 reflect the same secondary structures as those observed for untreated cells (Fig. 7c). On the contrary the second derivative spectra acquired from the map of cells treated with NM111 show a broader and nearly featureless main absorption band centered at 1552 $cm^{-1}$, suggesting the loss of a regular protein conformation.

Alterations concerning nucleic acids can be detected by analyzing the DNA backbone characteristic bands [35]. Generally, an increased density of hydrogen bonds is associated with a shift of the $PO_2$ asymmetric stretching from 1240 to 1220 $cm^{-1}$. Moreover, the occurrence of a pathological phosphorylation process is evidenced by an increased intensity of the corresponding bands. In order to evaluate the intensity

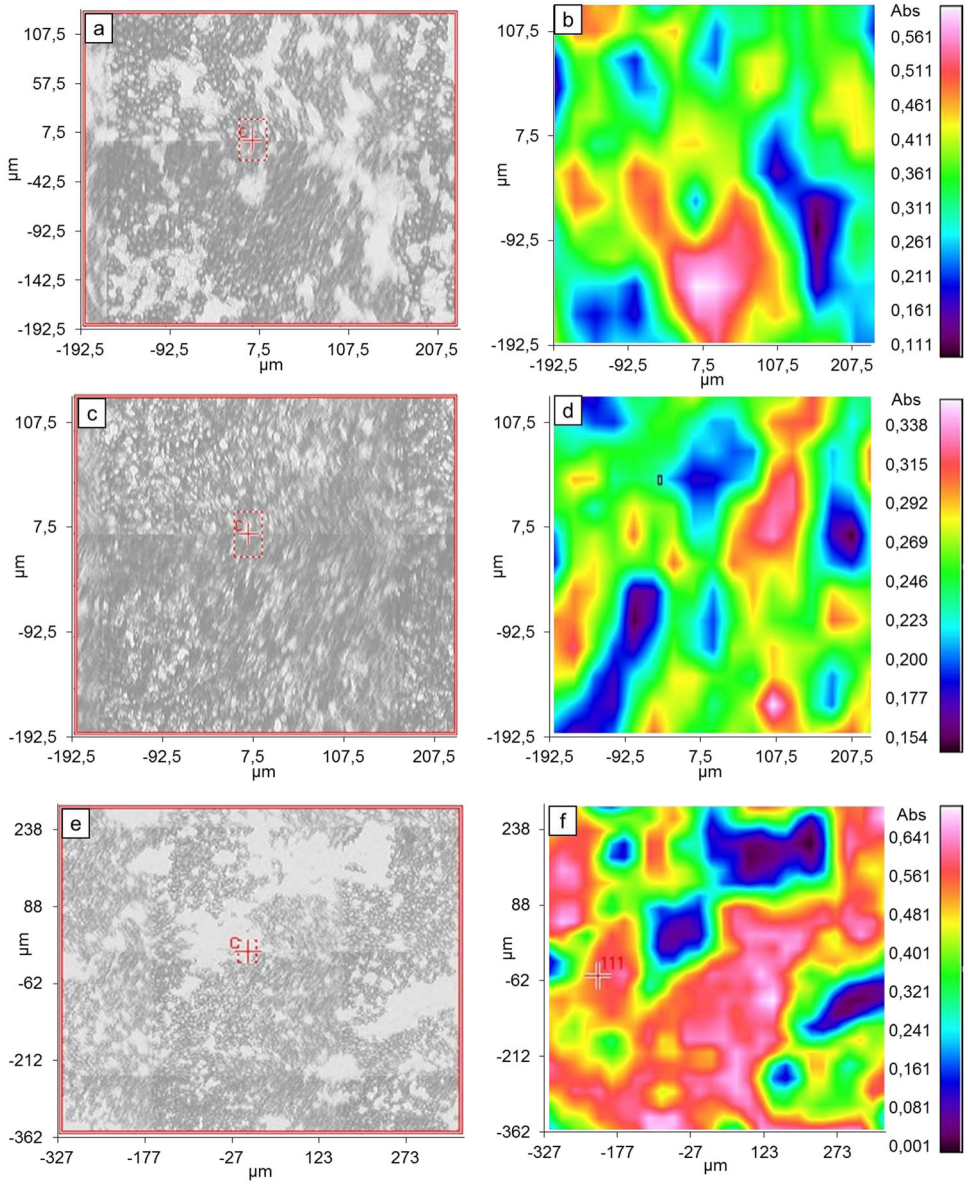


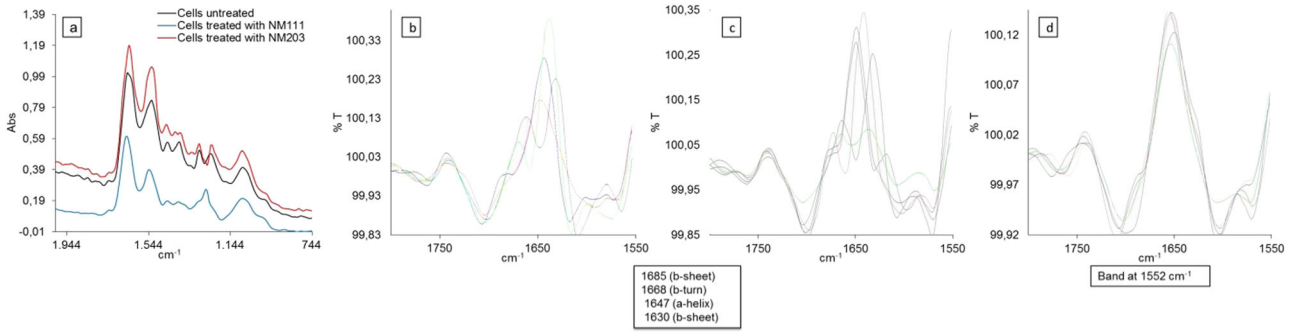


**Fig. 6** FTIR Chemical Imaging analysis was performed directly on the cells before and after 24 incubation with INMs at higher dose (100 µg/ml). The cells were seeded on a $BaF_2$ plate, air dried for 5 min and analyzed (sample $n = 3$, for each sample acquisition of at least 3 spectral maps). Optical images and corresponding chemical maps of untreated cells (**a, b**), cells treated with NM111 (**c, d**) and cells treated with NM203 (**e, f**)

**Fig. 7** Spectra of untreated cells and cells treated with NM111 and NM203 showing DNA spectral bands at 980–1149 $cm^{-1}$, $PO_2$ stretching vibrations at 1151–1350 $cm^{-1}$, amide I at 1600–1700 $cm^{-1}$ and amide II at about 1550 $cm^{-1}$ (**a**); second derivative spectra of amide I for untreated cells (**b**), cells treated with NM203, showing the typical secondary structure of proteins with bands at 1685 (β-sheet), 1668 (β-turn), 1647 (α-helix), and 1630 (β-sheet) $cm^{-1}$ (**c**) and cells treated with NM111, showing a broader absorption band centered at 1552 $cm^{-1}$, indicating the loss of a regular protein conformation (**d**)

**Table 2** Protein and DNA spectral bands for untreated cells, cells treated with NM111 (cells + NM111), and cells treated with NM203 (cells + NM203)

| | Amide I | Amide II | $PO_2$ asymmetric stretching | $PO_2$ symmetric stretching |
|---|---|---|---|---|
| untreated cells | 1649–1639 $cm^{-1}$ | 1530 $cm^{-1}$ | 1350–1150 $cm^{-1}$ variable | 1083–1086 $cm^{-1}$ |
| cells + NM111 | 1648 $cm^{-1}$ | 1540 $cm^{-1}$ | Variable | 1088–1075 $cm^{-1}$ |
| cells + NM203 | 1652–1642 $cm^{-1}$ | 1530 $cm^{-1}$ | Variable | 1084 $cm^{-1}$ |

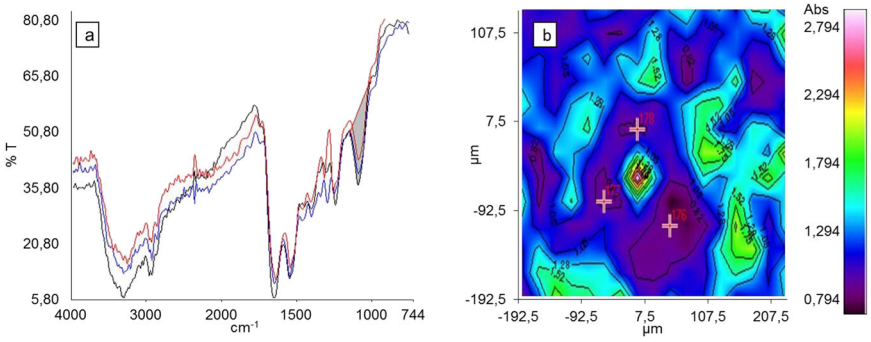


**Fig. 8** Representative spectra (**a**) and correlation map (**b**) as a function of nucleic acid (1144–1004 $cm^{-1}$)/amide II (1578–1480 $cm^{-1}$) band ratio for untreated cells. The same analysis was performed for identifying numerical variations of spectral markers for cells treated with either NM203 or NM111. The band values obtained for all the samples showed a possible alteration of nucleic acids only for the cells treated with NM111 at 100 µg/ml after 24 h incubation

variations, spectral maps as a function of band ratio between nucleic acids (1144–1004 $cm^{-1}$) and amide II (1578–1480 $cm^{-1}$) were acquired for untreated cells and cells treated with either NM203 or NM111. Figure 8 shows representative spectra and their corresponding correlation map recorded as function of such band ratio for untreated cells. By analyzing the numerical variations of spectral markers, the following band ratio values were obtained: R = (1144–1004)/(1578–1480) = 0.82, for untreated cells; R = (1144–1004)/(1578–1480) = 1.14–1.47, for cells treated with NM111 and R = (1144–988)/(1578–1480) = 0.82 for cells treated with NM203. These results are indicative of a possible alteration of nucleic acids only for the cells treated with zinc oxide INMs at the highest concentration after 24 h incubation, confirming the observations drawn from the results of the previously described analyses.

The combination of FTIR with Chemical Imaging allowed a fast and straightforward evaluation of modifications occurring in cellular biomolecules (i.e. nucleic acids, proteins) by comparative inspection of specific spectral profiles in normal and in altered conditions, the latter possibly induced by NMs. In addition, advanced analytical tools may be considered as an alternative strategy for hazard assessment in the direction of reducing in vivo experiments [14].

Concerning zinc oxide INMs, the presence of surface contaminants may affect their biosafety, although pure zinc oxide is considered as a very promising multifunctional material for medical applications. Thus the comprehensive concept of safer-by-design firstly includes the need for a careful selection of synthesis/production methods for NMs. In this respect, greener methods allowing the production of zinc oxide nanoparticles free of toxic contaminants could be of interest for improving the suitability of these nanomaterials for biomedicine and therapeutic applications [40, 41].

## 4 Conclusion

A comprehensive study to evaluate the two-way cell-nanomaterials interaction was performed, involving a combination of techniques to analyze the possible effects of the morphological, physico-chemical and biological features of such complex systems. Good agreement was observed among the results of MTS assay in several independent experiments for both NM203 and NM111. For all concentrations of NM203, high values of cell survival were found; on the contrary, a toxic effect exerted by NM111 on A549 cells was detected at high doses. The DLS analysis seems to indicate a poorer dimensional stability as a result of a higher tendency to aggregate after contact with culture medium for NM111 compared to NM203. The DLS analysis, carried out in parallel with MTS assay, suggests that nanometer size is not associated per se with cytotoxicity. Instead, a combination of factors including chemical nature, agglomeration state and, in particular, the presence of organic contaminants in NM111, as revealed by FTIR and GC–MS analyses, could explain the observed toxicity of NM111 at high doses. FTIR Chemical Imaging allowed the evaluation of possible alterations of protein secondary structure and nucleic acids in the cells treated with this zinc oxide nanomaterial at the highest concentration after 24 h incubation.

Overall, our results confirm the importance of developing new experimental methods and techniques for improving the knowledge about the biosafety of nanomaterials. Concerning already established in vitro biological assay, such as cell viability test, it is important to evaluate their suitability for testing nano-sized materials, by reducing possible interferences with test parameters. In addition, this study demonstrates the added value of an integrated methodology including well established methods and new advanced characterization techniques for evaluating nanotoxicity using the same in vitro human cell model and the same NM. Chemical Imaging was used for the first time, to the best of our knowledge, to identify molecular events induced either directly by nanomaterials or by their contaminants. This approach is very appealing since it gives biochemical information without the need of time-consuming indirect assays often leading to artifact issues.

Finally, the introduction of new complementary and advanced techniques such as FTIR Chemical Imaging and GC–MS improves our understanding of the interactions at the molecular level between cells and nanomaterials, and expands the testing protocols to be included in the toolbox for regulatory purposes.

**Acknowledgements** This research was partially funded by the European Union Seventh Framework Programme (FP7/2007-2013) under the project NANoREG (A common European approach to the regulatory testing of nano-materials), grant agreement 310584.

## Compliance with ethical standards

**Conflict of interest** The authors declare that they have no conflict of interest.

**Publisher's note** Springer Nature remains neutral with regard to jurisdictional claims in published maps and institutional affiliations.

## References

1. Peer D, Karp JM, Hong S, Farokhzad OC, Margalit R, Langer R. Nanocarriers as an emerging platform for cancer therapy. Nat Nanotechnol. 2007;2:751–60.
2. Duncan R. Polymer conjugates as anticancer nanomedicines. Nat Rev Cancer. 2006;6:688–701.
3. Ferrari M. Cancer nanotechnology: opportunities and challenges. Nat Rev Cancer. 2005;5:161–71.
4. Zhang L, Gu FX, Chan JM, Wang AZ, Langer RS, Farokhzad OC. Nanoparticles in medicine: therapeutic applications and developments. Clin Pharm Ther. 2008;83:761–9.
5. Tang L, Cheng J. Nonporous silica nanoparticles for nanomedicine application. Nano Today 2013;8:290–312.
6. Zhang H, Xia JY, Pang X, Zhao M, Wang B, Yang L et al. Magnetic nanoparticle-loaded electrospun polymeric nanofibers for tissue engineering. Mat Sci Eng C. 2017;73:537–43.
7. Panchal RG. Novel therapeutic strategies to selectively kill cancer cells. Biochem Pharmacol. 1998;55:247–52.
8. Nel A, Xia T, Madler L, Li N. Toxic potential of materials at the nanolevel. Science. 2006;311:622–7.
9. McNeil SE. Nanotechnology for the biologist. J Leukoc Biol. 2005;78:585–94.
10. Wagner V, Dullaart A, Bock AK, Zweck A. The emerging nanomedicine landscape. Nat Biotechnol. 2006;24:1211–7.
11. Hanley C, Layne J, Punnoose A, Reddy KM, Coombs I, Coombs A et al. Preferential killing of cancer cells and activated human T cells using zinc oxide nanoparticles. Nanotechnology. 2008;19:295103–13.
12. Wang H, Wingett D, Engelhard MH, Feris K, Reddy KM, Turner P et al. Fluorescent dye encapsulated ZnO particles with cell specific toxicity for potential use in biomedical applications. J Mater Sci Mater Med. 2009;20:11–22.
13. Zhang Y, Nayak Y, Tapas R, Hong H, Cai W. Biomedical Applications of Zinc Oxide Nanomaterials. Curr Mol Med. 2013;13:1633–45.
14. Accomasso L, Cristallini C, Giachino C. Risk assessment and risk minimization in nanomedicine: a need for predictive, alternative, and 3Rs strategies. Front Pharmacol. 2018;9:art 228.
15. Zhang Y, Nguyen KC, Lefebvre DE, Shwed PS, Crosthwait J, Bondy GS et al. Critical experimental parameters related to the cytotoxicity of zinc oxide nanoparticles. J Nanopart Res. 2014;16:24–40.
16. Gojova A, Guo B, Kota RS, Rutledge JC, Kennedy IM, Barakat AI. Induction of inflammation in vascular endothelial cells by metal oxide nanoparticles: effect of particle composition. Environ Health Perspect. 2007;115:403–9.
17. Reddy KM, Feris K, Bell J, Wingett DG, Hanley C, Punnoose A. Selective toxicity of zinc oxide nanoparticles to prokaryotic and eukaryotic systems. Appl Phys Lett. 2007;90:2139021–3.
18. Gil F, Pla A, Hernandez AF, Mercado JM, Mendez F. A fatal case following exposure to zinc chloride and hexachloroethane from a smoke bomb in a fire simulation at a school. Clin Toxicol. 2008;46:563–5.
19. Bengalli R, Gualtieri M, Capasso L, Urani C, Camatini M. Impact of zinc oxide nanoparticles on an in vitro model of the human air-blood barrier. Toxicol Lett. 2017;279:22–32.
20. Sahu D, Kannan GM, Vijayaraghavan R. Size-dependent effect of zinc oxide on toxicity and inflammatory potential of human monocytes. J Toxicol Environ Health A. 2014;77:177–91.
21. Wang B, Zhang J, Chen C, Xu G, Qin X, Hong Y et al. The size of zinc oxide nanoparticles controls its toxicity through impairing autophagic flux in A549 lung epithelial cells. Toxicol Lett. 2018;285:51–9.
22. Kim I-Y, Joachim E, Choi H, Kim K. Toxicity of Silica nanoparticles depends on size, dose, and cell type. Nanomedicine. 2015;11:1407–16.
23. Song MK, HS Lee HS, Choi HS, Shin CY, Kim YJ, Park YK et al. Octanal-induced inflammatory responses in cells relevant for lung toxicity: expression and release of cytokines in A549 human alveolar cells. Hum Exp Toxicol. 2014;33:710–21.
24. Totaro S, Cotogno G, Rasmussen K, Pianella F, Roncaglia M, Olsson H et al. The JRC nanomaterials repository: a unique facility providing representative test materials for nanoEHS research. Regul Toxicol Pharmacol. 2016;81:334–40.
25. Miller LM, Dumas P. From structure to cellular mechanism with infrared microspectroscopy. Curr Opin Struc Biol. 2010;20:649–56.
26. Singh C et al. NM-series of representative manufactured nanomaterials—zinc oxide NM-110, NM-111, NM-112, NM-113: characterisation and test item preparation, Luxembourg: Publications Office of the European Union; 2011. p. 141. EUR—Scientific and Technical Research series—ISSN 1831-9424 (online), ISSN 1018-5593 (print). https://doi.org/10.2787/55008.

27. Rama Narsimha Reddy A, Srividya L. Evaluation of in vitro cytotoxicity of zinc oxide (ZnO) nanoparticles using human cell lines. J Toxicol Risk Assess. 2018;4:009.
28. Ng CT, Yong LQ, Hande, Ong CN, Yu LE, Bay BH et al. Zinc oxide nanoprtcles exhibit cytotoxicity and genotoxicity through oxidative stress responses in human lung fibroblasts and *Drosophila Melanogasters*. Int J Nanomed. 2017;12:1621–37.
29. Monopoli MP, Walczyk D, Campbell A, Elia G, Lynch I, Bombelli FB et al. Physical-chemical aspects of protein corona: relevance to in vitro and in vivo biological impacts of nanoparticles. J Am Chem Soc. 2011;133:2525–34.
30. Ongena K, Das C, Smith JL, Gil S, Johnston G. Determining cell number during cell culture using the Scepter cell counter. J Vis Exp. 2010;45:e2204.
31. Tahara M, Inoue T, Miyakura Y, Horie H, Yasuda Y, Fujii H et al. Cell diameter measurements obtained with a handheld cell counter could be used as a surrogate marker of G2/M arrest and apoptosis in colon cancer cell lines exposed to SN-38. Biochem Biophys Res Commun. 2013;434:753–9.
32. Varaprath S, Larson PS. Degradation of monophenylheptamethylcyclotetrasiloxane and 2,6-cis-diphenylhexamethylcycloterasiloxane in Londo Soil. J Polym Environ. 2002;10:119–31.
33. Varaprath S, Salyers KL, Plotzke KP, Nanavati S. Identification of metabolites of octamethilcyclotetrasiloxane ($D_4$) in rat urine. Drug Metab Dispos. 1999;27:1267–73.
34. Song MK, Choi HS, Lee HS, Kim YJ, Park YK, Ryu JC. Analysis of microRNA and mRNA expression profiles highlights alterations in modulation of the MAPK pathway under octanal exposure. Environ Toxicol Pharmacol. 2014;37:84–94.
35. Mattson EC, Aboualizadeh E, Barabas ME, Stucky CL, Hirschmugl CJ. Opportunities for live cell FT-infrared imaging: macromolecule identification with 2D and 3D localization. Int J Mol Sci. 2013;14:22753–81.
36. Lipiec E, Kowalska J, Lekki J, Wiechec A, Kwiatek WM. FTIR microspectroscopy in studies of DNA damage induced by proton microbeam in single PC-3 Cells. Acta Phys Pol A. 2012;2:506–9.
37. Singh B, Gautam R, Kumor S, Vinaykumar BN, Nongthomba U, Nandi D et al. Application of vibrational microspectroscopy to biology and medicine. Curr Sci. 2012;102:232–44.
38. Falahat R, Wiranowska M, Toomeya R, Alcantar N. ATR-FTIR analysis of spectral and biochemical changes in glioma cells induced by chlorotoxin. Vib Spectrosc. 2016;87:164–72.
39. Mourant JR, Gibson RR, Johnson TM, Carpenter S, Short KW, Yamada YR et al. Methods for measuring the infrared spectra of biological cells. Phys Med Biol. 2003;48:243–57.
40. Mirzaei H, Darroudi M. Zinc oxide nanoparticles: biological synthesis and biomedical applications. Ceram Int. 2017;43:907–14.
41. Darroudi M, Sabouri Z, Oskuee RK, Zak AK, Kargar H, Hamid MHNA. Green chemistry approach for the synthesis of ZnO nanopowders and their cytotoxic effects. Ceram Int. 2014; 40:4827–31.